Experimental and Updated Kinetic Modeling Study of Neopentane Low Temperature Oxidation

Bingzhi Liu, Shijun Dong, Janney Debleza, Weiye Chen, Qiang Xu, Hong Wang, Jérémy Bourgalais, Olivier Herbinet, Henry Curran, Frédérique Battin-Leclerc, et al.

Experimental and Updated Kinetic Modeling Study of Neopentane Low Temperature Oxidation

Bingzhi Liu [a], Shijun Dong [b, d], Janney Debleza [c], Weiye Chen [a], Qiang Xu [a], Hong Wang [a], Jérémy Bourgalais [c], Olivier Herbinet [c], Henry J. Curran [b], Frédérique Battin-Leclerc [c], Zhandong Wang [a, e*]

[a] *National Synchrotron Radiation Laboratory, University of Science and Technology of China, Hefei, Anhui 230029, PR China*

[b] *Combustion Chemistry Centre, School of Chemistry, Ryan Institute, MaREI, NUI Galway H91TK33, Ireland*

[c] *Université de Lorraine, CNRS, LRGP, F-54000 Nancy, France.Laboratoire*

[d] *School of Energy and Power Engineering, Huazhong University of Science and Technology, Wuhan, Hubei 430074, PR China*

[e] *State Key Laboratory of Fire Science, University of Science and Technology of China, Hefei, Anhui 230026, PR China*

Published in J. Phys. Chem. A 2023, 127, 9, 2113–2122

10.1021/acs.jpca.2c03795

Abstract: Neopentane is an ideal fuel model to study low temperature oxidation chemistry. The significant discrepancies between experimental data and simulations using the existing neopentane models indicate that an updated study of neopentane oxidation is needed. In this work, neopentane oxidation experiments are carried out using two jet-stirred reactors (JSRs) at 1 atm, at a residence time of 3 s, and at three different equivalence ratios of 0.5, 0.9, and 1.62. Two different analytical methods (synchrotron vacuum ultraviolet photoionization mass spectrometry and gas chromatography) were used to investigate the species distributions. Numerous oxidation intermediates were detected and quantified, including acetone, 3,3-dimethyloxetane, methacrolein, isobutene, 2-methylpropanal, iso-butyric acid, and the peroxides, which are valuable for validating the kinetic model describing neopentane oxidation. In the model development, the pressure dependence of the reaction classes of $\dot{Q}OOH + O_2$ and $\dot{Q}OOH$ decompositions are considered, which improves the prediction of the low temperature oxidation reactivity of neopentane. Another focus of model development is to improve the prediction of carboxylic acids during the low temperature oxidation of neopentane. The detection and identification of iso-butyric acid indicates the existence of the Korcek mechanism during neopentane

* Corresponding author: E-mail: zhdwang@ustc.edu.cn (Z. Wang)

oxidation. Regarding the formation of acetic acid, the reaction channels are considered to be initiated from the reactions of ȮH radical addition to acetaldehyde/acetone. This updated kinetic model is validated extensively against the experimental data in this work and various experimental data available in the literature, including ignition delay times (IDTs) from both shock tubes (STs) and rapid compression machines (RCMs) and JSR speciation data at high temperatures.

Keywords: neopentane oxidation; kinetic modeling; Korcek mechanism; carboxylic acids; synchrotron vacuum ultraviolet photoionization mass spectrometry

1. Introduction

Considering energy resources, combustion efficiency, and the strict control of pollutant emissions, further exploration of combustion chemistry and the development of advanced combustion technology is of contemporary significance.[1] To achieve cleaner combustion, new engine strategies[2-5] are developing rapidly. In particular, low temperature combustion (LTC) has recently attracted great interest.[3-5] LTC is a combustion strategy for advanced internal combustion engines (ICEs), including homogeneous charge compression ignition (HCCI),[4] reactivity-controlled compression ignition (RCCI),[3] and premixed charge compression ignition (PCCI),[6,7] which has great advantages in simultaneously reducing pollutant emissions and improving combustion efficiency. However, LTC is currently facing many design and research challenges that require the support of numerical calculations and computational fluid dynamics (CFD) simulations.[5] Consequently, further studies on fuel chemistry and establishing precise detailed combustion kinetic models is one of the prerequisites.

The low temperature oxidation of large alkanes is governed by successive radical additions to O_2 and intramolecular H-atom migration reactions. The reaction scheme leads to many oxygenated species and makes the low temperature oxidation reaction networks particularly complex, especially when the mechanism of the 3rd addition to O_2 is explored and added.[8-12] Neopentane (2,2-dimethyl propane) is one of the unique representatives of branched alkanes with a symmetrical molecular structure and only identical H-atoms and thus gives a single alkyl radical by H-atom abstraction reactions. This leads to a more concise low temperature oxidation network. Accordingly, neopentane is an ideal model fuel to study low temperature oxidation chemistry and to develop detailed kinetic models of alkanes.

Some early work[13-16] conducted preliminary explorations on the reaction mechanism of neopentane. Recently, Bugler et al.[17,18] provided the latest ignition delay time (IDT) results of the pentane isomers and proposed a detailed model in which the thermodynamic data were systematically updated and consistent rate rules were used for the important reaction classes. Eskola et al.[19] used synchrotron vacuum ultraviolet photoionization mass spectrometry (SVUV-PIMS) combined with a

flow reactor to explore the oxidation products of neopentane in the temperature range of 550–675 K; the potential intermediates from keto-hydroperoxide (KHP) decomposition were discussed. Hansen et al.[20] conducted low temperature oxidation experiments of neopentane using a jet-stirred reactor (JSR) and a time-resolved flow reactor. KHP and keto-dihydroperoxide (KDHP) species were detected. They developed a kinetic model including the 3rd O_2 addition reaction network based on the model of Bugler et al.[17,18] to explore the effect of the 3rd O_2 addition reactions on IDTs. Very recently, neopentane oxidation in JSRs was studied at 1 atm in the temperature range of 500–850 K and φ = 0.5 by Bourgalais et al.,[21] and the products were analyzed via a combined theoretical, chromatographic, mass spectrometric, and photoelectron photoion coincidence spectroscopy (PEPICO) study. Although the current neopentane kinetic models in the literature have been validated extensively, discrepancies between the measured and predicted neopentane reactivity, as well as mole fractions of many important species still exist, such as 2-methylpropanal ($(CH_3)_2CHCH=O$), 3,3-dimethyloxetane ($CH_3C(CH_2OCH_2)CH_3$), acetone (CH_3COCH_3), isobutene ($(CH_3)_2C=CH_2$), and methacrolein ($CH_3C(=CH_2)CH=O$). The new JSR experimental data and the corresponding analyses in the work of Bourgalais et al.[21] show that the existing neopentane models need to be improved. These latest works[17-21] provide a starting point and valuable references for the further extension and improvement of the neopentane kinetic model.

In this work, SVUV-PIMS combined with gas chromatography (GC) was used to detect and quantify the key intermediates and final products of neopentane oxidation in JSRs at 1 atm and at equivalence ratios of 0.5, 0.9, and 1.62. Important oxidation intermediates, e.g., acetone, 3,3-dimethyloxetane, methacrolein, isobutene, 2-methylpropanal, and iso-butyric acid ($(CH_3)_2CHC(=O)OH$), were identified and quantified, which are crucial to clarify the low temperature oxidation mechanism of neopentane and to refine and develop the kinetic model. Next, the rate constants of key reaction classes in the neopentane submechanism, e.g., the reaction classes of $\dot{Q}OOH + O_2$ and $\dot{Q}OOH$ decompositions, were re-examined and evaluated based on new JSR experimental data and available studies in the literature. Furthermore, carboxylic acid formation chemistry was

revisited. The Korcek mechanism was added, and the rate constants for the reactions of ȮH radical addition to acetaldehyde were updated. The reaction pathways of ȮH radical addition to acetone and subsequent decomposition were proposed to better predict the acetic acid mole fraction distribution. This updated model satisfactorily predicts current experimental data and various experimental data available in the literature.

2. Experimental method

In this work, we carried out neopentane oxidation experiments in two JSRs using the analytical methods of SVUV-PIMS and GC. The results obtained by different analytic methods are mutually verified and supplemented. The diluent gas used in the JSR-SVUV-PIMS experiment was argon (Ar), while the diluent gas used in the JSR-GC experiment was helium (He). The influence of different dilution gases on the experimental results is negligible. The initial concentration of neopentane in all experiments was 0.015, and the residence time was 3 s. The detailed JSR experimental conditions are summarized in Table 1.

2.1 The JSR experiments based on SVUV-PIMS

The first experimental work was carried out in NSRL (Hefei, China). The specific description of this experimental platform can be found in recent work.[22] Gaseous neopentane (purity 99.8%) is mixed with diluent gas (Ar) and oxygen and enters the JSR. There are four nozzles with a diameter of 0.3 mm in the sphere of the JSR. The gas mixture forms jets through the four nozzles and is evenly mixed in the reactor. The mixture is sampled by the tapered quartz nozzle that is welded on the JSR sphere to form a molecular beam, which is ionized by the SVUV-PIMS. The mass resolution (m/Δm) of SVUV-PIMS was ~4000 at m/z 72 in this experiment. Methods of species identification and quantification can be found in previous work.[23] The photoionization cross-sections (PICSs) are obtained from an online database,[24] available literature data,[25-27] and experimental measurements in this work. The uncertainties of the measured mole fractions are within ± 10% for neopentane and oxygen, ± 20% for species with known PICSs, and a factor of two for those with estimated PICSs.

2.2 The JSR experiments based on GC

JSR experiments under the same conditions were also carried out in LRGP (Nancy, France) using an analytical method based on online GC-FID/GC-MS. A detailed description of the experimental setup can be found in previous publications.[23,27,28] The outlet of the JSR is connected to two GCs through a heated transfer line.[23,27] The first GC is equipped with a Carbosphere packed column and a thermal conductivity detector (TCD) that allows the acquisition of the mole fraction distributions of H_2, O_2, CO, and CO_2. The second GC is equipped with a PlotQ capillary column and a flame ionization detector (FID) to quantify molecules ranging from methane to reaction products containing up to five carbon atoms and one or two oxygen atoms.[23,27] The mass spectrometer (MS) analyser was adopted for the identification of reaction products according to the NIST Mass Spectrometry database. For O_2, CH_4, CO, CO_2, and some common hydrocarbons, standard gases were used for TCD and FID calibration. For other species detected by FID, the effective carbon number (ECN) method was used for quantification. The uncertainties of the species mole fractions calculated using the standard gas are within ± 5%, while those obtained using the ECN method are ± 10%.

Table 1. The JSR experimental conditions in this work

Location	T (K)	*p* (bar)	τ (s)	φ	neopentane	O_2	He/Ar
NSRL	500–825	1.03	3	0.5	0.015	0.24	0.745
NSRL	500–825	1.03	3	0.9	0.015	0.133	0.852
NSRL	500–825	1.03	3	1.62	0.015	0.0741	0.9109
LRGP	500–825	1.07	3	0.5	0.015	0.24	0.745
LRGP	500–1100	1.07	3	0.9	0.015	0.133	0.852
LRGP	500–1100	1.07	3	1.62	0.015	0.0741	0.9109

3. Kinetic model development

The current model is developed based on NUIGMech1.2[29] and the previously published pentane mechanism.[17] The submechanisms of the three pentane isomers were developed using consistent rate rules and thermochemistry.[17] The neopentane subchemistry was well validated against various experimental data, including IDTs measured in STs and RCMs and some JSR species data measured

at high temperatures. Since the new JSR data of this study mainly focused on neopentane oxidation in the low temperature regime, the model updates mainly focused on the low temperature chemistry of neopentane submechanism.

In this study, one of the major updates in the neopentane submechanism is adding pressure-dependent rate constants for the reaction classes of $\dot{Q}OOH + O_2$ and $\dot{Q}OOH$ decompositions. These reaction classes are critically important for alkane low temperature chemistry, as the rate constants directly controlled the branching ratios of chain propagation and chain branching pathways. In the previous pentane mechanism,[17] only high-pressure limits were used for these reaction classes. However, the high-pressure limits are slightly too fast to simulate JSR oxidation at 1 atm. Goldsmith et al.[30] theoretically investigated the kinetics of the O_2 + propyl system, highlighting the pressure-dependent reaction rate coefficients of the $\dot{Q}OOH$ radicals. Recently, Duan et al.[31,32] also performed theoretical studies of the rate constants of O_2 addition to n-butyl and four heptyl radicals, with significant pressure dependence observed above ca. 500 K. In the current model, the rate constants at 1 atm for both $\dot{Q}OOH + O_2$ and $\dot{Q}OOH$ decompositions are included and are a factor of two slower than the high-pressure limit values across the temperature range. The rate constants of these reactions are assumed to reach the high-pressure limits at pressures of 10 atm and higher.

Other major updates of the current mechanism include the new formation reaction pathways of carboxylic acids. In this work, formic acid, acetic acid, and iso-butyric acid were measured. In previous studies,[33-35] it was suggested that carboxylic acids are mainly formed via the Korcek mechanism, i.e., the decomposition of γ-keto hydropeoxide (γ-KHP) species. Scheme 1 shows the Korcek mechanism for neopentane proposed by Eskola et al.[19] γ-KHP undergoes cyclic peroxide isomerization that leads to two aldehydes (formaldehyde and 2-methylpropanal) and two acids (formic acid and iso-butyric acid). The rate constants for the Korcek mechanism of the C_5 KHP are adopted to be the same as the Korcek reaction of C_3 KHP calculated by Goldsmith et al.[36], with an assumption that the extra methyl groups in the C_5 KHP (3-hydroperoxy-2,2-dimethylpropanal) are spectators. In addition, the reactions of $\dot{O}H$ radical additions to formaldehyde/acetaldehyde and subsequent reactions can also lead to the

formation of formic acid, as shown in Scheme 2. In NUIGMech1.2,[29] the rate constant of ȮH radical addition to formaldehyde and the subsequent decomposition of the adduct to formic acid were adopted from the work of Xu et al.[37] In this work, the rate constant of ȮH radical addition to acetaldehyde is determined to be the same as the reaction of ȮH radical addition to formaldehyde. For the decomposition of the adduct to formic acid via β-C-C bond scission, the rate constant was estimated based on the decomposition of the isopropoxy radical.[38]

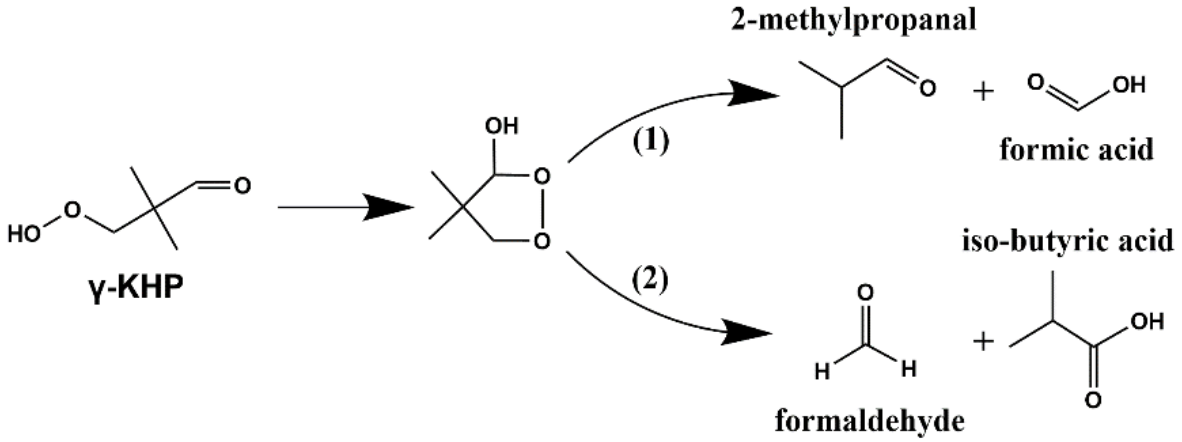

Scheme 1 The γ-KHP decomposition of neopentane via the Korcek mechanism.[33]

ȮH radical addition to acetaldehyde and the subsequent scission of the C–H bond could lead to the formation of acetic acid, as shown in Scheme 2. In addition, we propose another pathway that occurs via ȮH radical addition to acetone and the subsequent decomposition, producing a methyl radical and acetic acid. The branching ratio of ȮH addition to acetone has been discussed in a number of studies.[39-41] It is suggested that this reaction pathway is slower than H-atom abstraction from acetone. However, as acetone is one of the major products of neopentane oxidation, the reaction pathways of ȮH radical addition to acetone and subsequent decomposition may be important in the prediction of acetic acid. In this study, the rate constant of ȮH addition to acetone was estimated by analogy with ȮH addition to formaldehyde,[37] with the activation energy decreasing by 2 kcal/mol, considering the structural difference between formaldehyde and acetone. Furthermore, the rate constants of the adduct decomposition of ȮH addition to acetone were estimated by analogy with the β-C–C bond scission of the isopropoxy radical.[38]

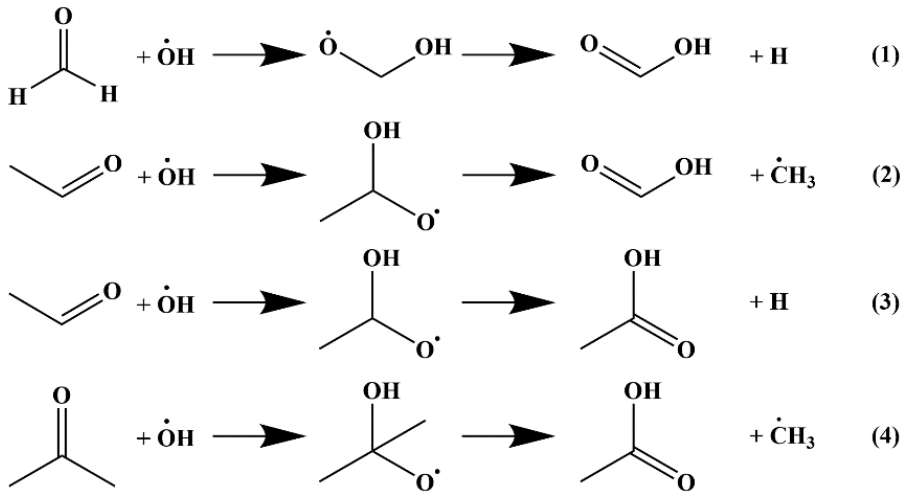

Scheme 2 The formation reaction pathways of formic acid and acetic acid by the ȮH radical addition to aldehydes and ketone in the model.

4. Results and discussion

4.1 Species measurement and quantification

Some important intermediates (acetone, formaldehyde, 3,3-dimethyloxetane, methacrolein, isobutene) were detected by both SVUV-PIMS and GC. Carbon monoxide and methane were measured by GC, and water was measured by SVUV-PIMS. Additionally, peroxides (hydrogen peroxide and methyl peroxide), carboxylic acids (formic acid, acetic acid, and iso-butyric acid), and alcohols (methanol) were detected, identified, and quantified by SVUV-PIMS. The PICSs of formaldehyde, hydrogen peroxide, acetic acid, and methyl peroxide were adopted from the literature studies.[25-27,42] The PICS of iso-butyric acid was measured in this work. Details of the PICS measurement method can be found in previous work,[43] and the table of PICS for iso-butyric is provided in the *Supplementary material*. The PICSs used for other species are from the online database.[24]

3,3-Dimethyloxetane is a critically important intermediate in the chain-propagation process. Eskola et al.[19] carried out time-resolved measurement and analysis on this intermediate. The PICS of 3,3-dimethyloxetane at the parent ion m/z 86.07 is very small (the maximum PICS at 9.5–11.0 eV is ~0.007 Mb), but it has a very large PICS at its daughter ion m/z 56.06.[19] For SVUV-PIMS, 3,3-dimethyloxetane was quantified by the PICS of the daughter ion m/z 56.06 at 9.8 eV. We note that isobutene also contributed a signal at m/z 56.06, so the signal of isobutene needed to be subtracted to

obtain the mole fraction of 3,3-dimethyloxetane. In this subtraction, we first obtain the mole fraction of isobutene at 9.3 eV. We note that the appearance energy for the daughter ion m/z 56.06 of 3,3-dimethyloxetane is ~9.45 eV, while the ionization energy for isobutene is ~9.2 eV. The photon energy of 9.3 eV could exclude the strong interference of the daughter ion of 3,3-dimethyloxetane. Here, we used 1,3-butadiene as a reference to obtain the mole fraction of isobutene at 9.3 eV. Considering the low PICS of isobutene at 9.3 eV, the uncertainty in its mole fraction is estimated to be ± 50%. Then, the mole fraction of 3,3-dimethyloxetane was quantified at 9.8 eV after subtracting the isobutene signal. Considering the impact of error propagation, the mole fraction uncertainty of 3,3-dimethyloxetane is also estimated to be ± 50%.

Two C_5 peroxides were measured in this work, i.e., the C_5 ROOH ($C_5H_{12}O_2$) and the C_5 KHP ($C_5H_{10}O_3$). They could be determined to be neopentyl hydroperoxide and 3-hydroperoxy-2,2-dimethylpropanal due to the highly symmetrical structure of neopentane. The C_5 KHP was also identified as 3-hydroperoxy-2,2-dimethylpropanal ($(CH_3)_2C(CH_2O_2H)CH=O$) by the ionization energy calculated by Hansen et al.[20]

4.2 Low temperature chemistry of neopentane

CHEMKIN PRO software[44] was used to simulate these JSR data. The measured and model-predicted mole fraction distributions of neopentane oxidation products are shown in Figs. 1-4 and Figs. S1-S4. Figure 1 shows the mole fraction profiles of neopentane, oxygen, carbon monoxide and water at φ = 0.5, φ = 0.9 and φ = 1.62, respectively. The neopentane model updated in this work can satisfactorily capture the profiles of reactants and final products at different equivalence ratios and different temperatures, especially under fuel-rich conditions.

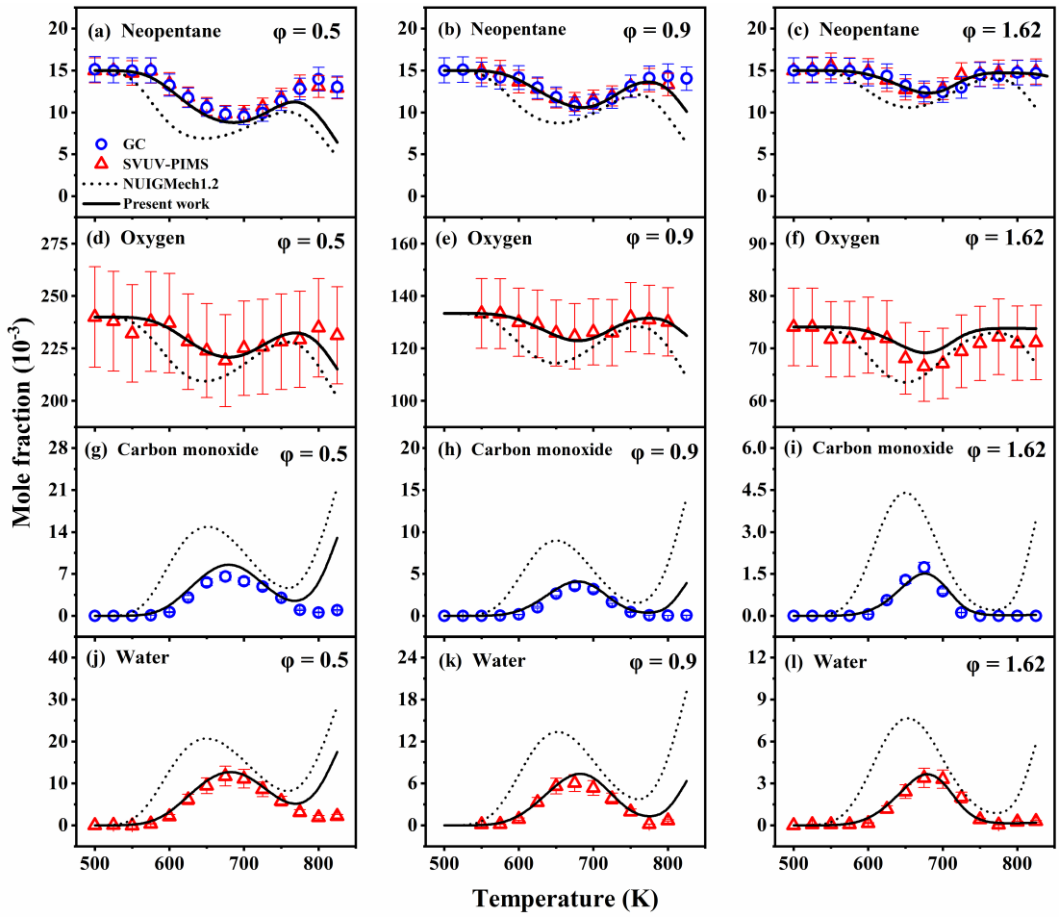

Figure 1 Measured (symbols) and model-predicted (lines) mole fraction profiles of neopentane, oxygen, carbon monoxide and water at φ = 0.5, φ = 0.9 and φ = 1.62. Dotted and solid lines represent the results predicted by NUIGMech1.2[29] and the present model, respectively. The error bar for the experimental data is given.

Under the three experimental conditions presented in Fig. 1, both the experimental and model-predicted results show significant low temperature reactivity and a notable negative temperature coefficient (NTC) zone. The reactivity of neopentane decreases as the equivalent ratio increases. NUIGMech1.2[29] overpredicts neopentane reactivity in the temperature range 550–675 K, while the model updated in this work can satisfactorily predict the reactivity. However, both models overpredict fuel reactivity in the temperature range of 750–850 K for φ = 0.5 and φ = 0.9. The overprediction is more evident at φ = 0.5. These major products formed during oxidation are also overpredicted at φ = 0.9, as seen in Figs. S1–S4 in the temperature range of 750–900 K. In contrast to the observation in this work, the models predicted the high temperature reactivity of neopentane well, as shown in Figs. S5–S7, with a much lower fuel initial mole fraction of 0.001 that was measured by Dagaut et al.[16] The sensitivity analyses in Fig. S8 indicate that some of the most sensitive reactions are related to the base

chemistry, and it is believed that future updates of base chemistry will improve the model predictions in the intermediate range (above 750 K).

The final products of the low temperature oxidation of neopentane are carbon monoxide and water. The GC method failed to detect carbon dioxide at 500–800 K, although the maximum carbon dioxide concentration predicted by the present model is ca. 500 ppm at 500–800 K and at φ = 0.5. The comparisons of the experimental and simulated results for oxygen, carbon monoxide, and water at φ = 0.5, φ = 0.9, and φ = 1.62 are also presented in Fig. 1. Considering the experimental error and model uncertainty, the updated model satisfactorily predicts the reactants and final products of the low temperature oxidation of neopentane.

In the following discussion on the oxidation intermediates, we will focus on the results at the experimental condition of φ = 0.5, and the results at other conditions of φ = 0.9 and φ = 1.62 are presented in the *Supplementary material*.

4.2.1 The first and second additions to O_2

Neopentane oxidation is initiated by H-atom abstraction initially by O_2 and subsequently by ȮH radicals to form neopentyl radicals (Ṙ). These radicals add to O_2 to form the neopentyl peroxy radical ($R\dot{O}_2$). Thereafter, a dominant reaction channel is the isomerization of $R\dot{O}_2$ radicals to hydroperoxy neopentyl radicals (ĊOOH) via a 6-membered ring transition state. The fate of ĊOOH radicals is critical for the low temperature chemistry of alkanes because they directly control the branching ratios of the chain-propagation and chain-branching pathways. In NUIGMech1.2,[29] the high-pressure limit rate constants of the first (Ṙ) addition to the O_2 reaction calculated by Miyoshi et al.[45] were used. The rate constants of the second (ĊOOH) addition to the O_2 reaction were based on the first Ṙ addition to the O_2 rate constants, with the A-factor decreasing by a factor of two based on the suggestions of Goldsmith et al.[30,46] The rate constant of the ĊOOH decomposition is derived from the rate rule of the LLNL model.[47] The pressure dependence of the reaction classes of ĊOOH + O_2 and ĊOOH decompositions, as described in Section 3, is considered by this model to satisfactorily capture the neopentane low temperature oxidation reactivity at 550–675 K.

Isobutene and 3,3-dimethyloxetane are the predominant species during neopentane low temperature oxidation. This is because the $R\dot{O}_2$ radical does not have any β-hydrogen and lacks the reaction pathway of concerted elimination that leads to olefins and $H\dot{O}_2$ radicals. Instead, the $R\dot{O}_2$ radicals dominantly isomerize to $\dot{Q}OOH$ radicals, which can either decompose to form 3,3-dimethyloxetane and an ȮH radical or undergo β-scission to form isobutene, ȮH and formaldehyde; formaldehyde is the byproduct in the formation of isobutene. These two reaction channels compete with each other, and the formation of isobutene and 3,3-dimethyloxetane inhibits the chain-branching process, which is directly related to the low temperature reactivity of neopentane. Furthermore, the $R\dot{O}_2$ radical derived from the first addition to O_2 reacts with $H\dot{O}_2$ radicals and leads to the formation of neopentyl hydroperoxide (ROOH). The second additions of $\dot{Q}OOH$ radicals to O_2 lead to peroxy neopentyl hydroperoxide radicals (ȮOQOOH), which leads to C_5 KHP and ȮH radicals via internal H-migration reactions. ROOH and C_5 KHP are the key intermediates formed by the first and second additions to O_2 reactions, and their decomposition is crucially important for the low temperature reactivity of neopentane.

Figure 2 presents the measured and model-predicted mole fraction profiles of 3,3-dimethyloxetane and isobutene at $\varphi = 0.5$. Considering the uncertainties of the SVUV-PIMS and GC measurements, the mole fractions of 3,3-dimethyloxetane and isobutene obtained by these two methods are in good agreement. The normalized signal and model-predicted profiles of ROOH and C_5 KHP are also presented here. ROOH and C_5 KHP were obtained by SVUV-PIMS, but they could not be quantified due to the lack of PICSs. The model developed in this work captures the mole fraction distributions of isobutene and 3,3-dimethyloxetane well and satisfactorily predicts ROOH and C_5 KHP formation and decomposition in the temperature range 500–800 K.

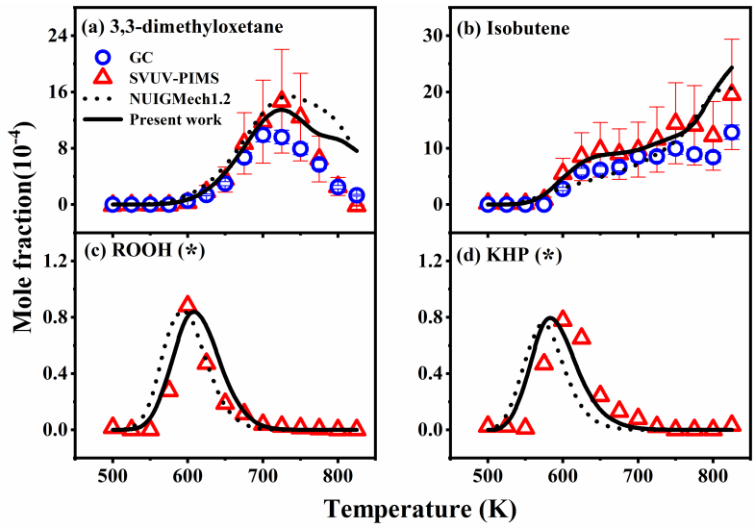

Figure 2 Measured (symbols) and model-predicted (lines) mole fraction profiles of 3,3-dimethyloxetane and isobutene at $\varphi = 0.5$ in neopentane low temperature oxidation. The signal profiles (*) of ROOH and KHP are also presented with a comparison of the profile shape from model prediction. The dotted and solid lines represent the results predicted by NUIGMech1.2[29] and the present model, respectively. The error bar for the experimental data is given.

4.2.2 C_5 KHP decomposition

The dominant KHP consumption pathway is the formation of ȮH radicals and keto alkoxy radicals through O–OH bond scission. The keto alkoxy radical leads to the formation of acetone via CH_2O loss and the following reactions in Scheme 3. Acetone is one of the dominant products during the low temperature oxidation of neopentane. These reaction channels are one of the main sources for the formation of acetone and formaldehyde. The kinetic model updated in this work predicts the formation of these two intermediates well, as shown in Fig. 3 and Fig. S1.

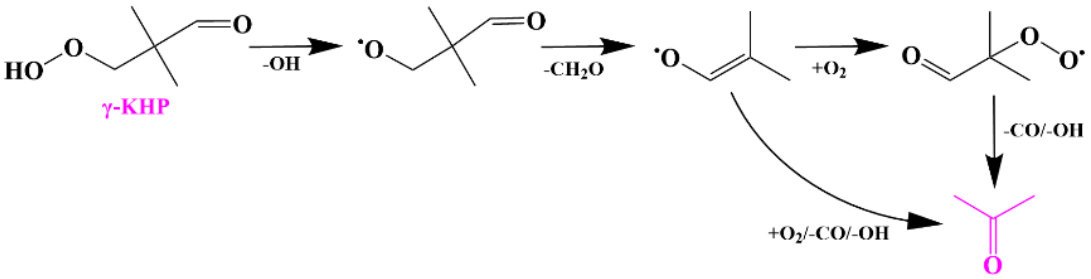

Scheme 3 The formation reaction pathways of acetone via C_5 KHP decomposition.

In addition to the above pathways of KHP unimolecular ȮH-loss and subsequent reactions, another potential pathway of KHP is decomposition via the Korcek mechanism,[33] which is known to

lead to a carbonyl compound and a carboxylic acid. The first decomposition pathway, Scheme 1 (1), of the Korcek reaction leads to the formation of 2-methylpropanal and formic acid. 2-Methylpropanal was detected and identified using GC and SVUV-PIMS, and formic acid was detected and identified using SVUV-PIMS. The second decomposition pathway, Scheme 1 (2), leads to the formation of formaldehyde and iso-butyric acid. Eskola et al.[19] observed a very weak product signal at m/z 88.05 during neopentane oxidation but could not identify its structure. Bourgalais et al.[21] obtained photoionization efficiency (PIE) spectra for m/z 88.05 during neopentane oxidation at 600 K and φ = 0.5. Their results suggested that the signal of m/z 88.05 came from 3-hydroperoxybut-1-ene. In this work, a PIE experiment was performed at 675 K and at φ = 0.9, and the results support the existence of iso-butyric acid. The signal of m/z 88.05 can be attributed to the combined contribution of iso-butyric acid and 3-hydroperoxybut-1-ene, as shown in Fig. S9. The comparison of the measured PIE curve with that of iso-butyric acid indicates that iso-butyric acid is the dominant contributor for m/z 88.05 at 675 K. The measured absolute PICS of iso-butyric acid is presented in Fig. S10.

The detection and identification of 2-methylpropanal, formic acid, formaldehyde, and iso-butyric acid indicate the existence of the Korcek reaction during neopentane oxidation. Their mole fraction profiles are presented in Fig. 3. We note that for 2-methylpropanal, the SVUV-PIMS data are significantly higher than the GC measurements. The reason for these discrepancies has been discussed in detail by Bourgalais et al,[21] i.e., SVUV-PIMS results were affected by the additional contributions from other isomers at m/z 72.06. These isomers can be well separated by the GC method; only GC data are shown here for better comparison with model-predicted results. For iso-butyric acid, the calculated mole fraction should have the contribution of 3-hydroperoxybut-1-ene, but the PIE comparison indicates that the contribution is not significant.

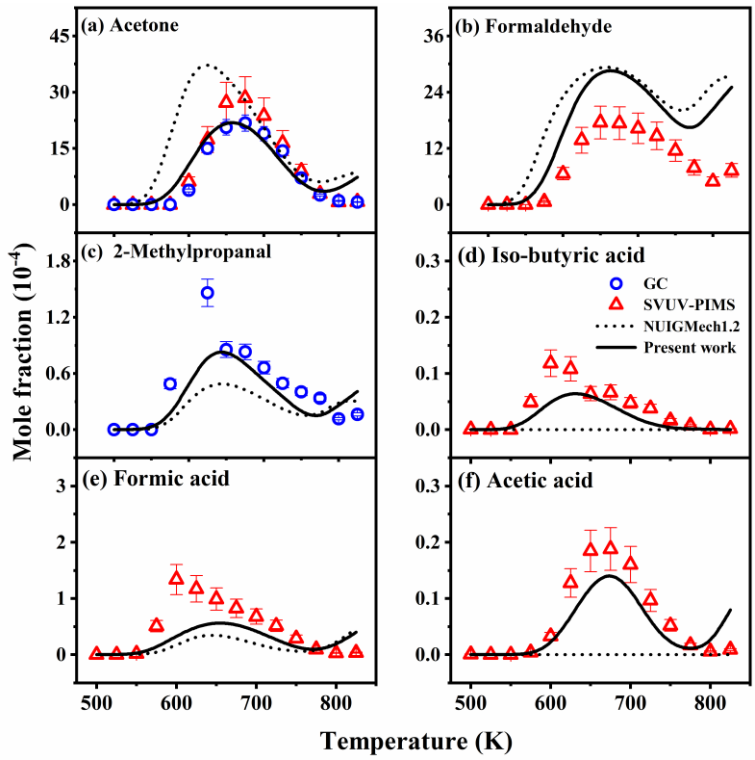

Figure 3 Measured (symbols) and model-predicted (lines) mole fraction profiles of acetone, formaldehyde, 2-methylpropanal, iso-butyric acid, formic acid, and acetic acid at $\varphi = 0.5$. The dotted and solid lines represent the results predicted by NUIGMech1.2[29] and the present model, respectively. The error bar for the experimental data is given.

It can be seen that their relative ratio is not in accord with the ratio from the Korcek decomposition in Scheme 1. The mole fraction of formaldehyde is much higher than that of iso-butyric acid. As discussed above, formaldehyde comes from other pathways, such as the pathway in Scheme 3. For 2-methylpropanal and formic acid, their mole fractions are close to each other. However, apart from formaldehyde, the model underpredicts the mole fraction of 2-methylpropanal, iso-butyric acid, and especially formic acid. The reaction pathway analysis for these three intermediates at $\varphi = 0.5$ and 650 K is shown in Scheme 4. For 2-methylpropanal, the main formation pathway is ȮH radical addition to isobutene and the subsequent reactions, with only a small contribution (~15%) from Korcek decomposition of the C_5 γ-KHP. For the formation of formic acid, the Korcek reaction channel of C_5 γ-KHP contributed ~52%, followed by the subsequent reaction of isobutene (~36%) and formaldehyde (~12%). For iso-butyric acid, the Korcek decomposition of C_5 γ-KHP is the only channel for its formation in the model. The above discussion indicates that Korcek decomposition is a source of

carboxylic acid, but they could not fully explain their formation, such as formic acid and iso-butyric acid. The underestimation of the rate constant for the Korcek decomposition may also be a potential explanation for the discrepancy.

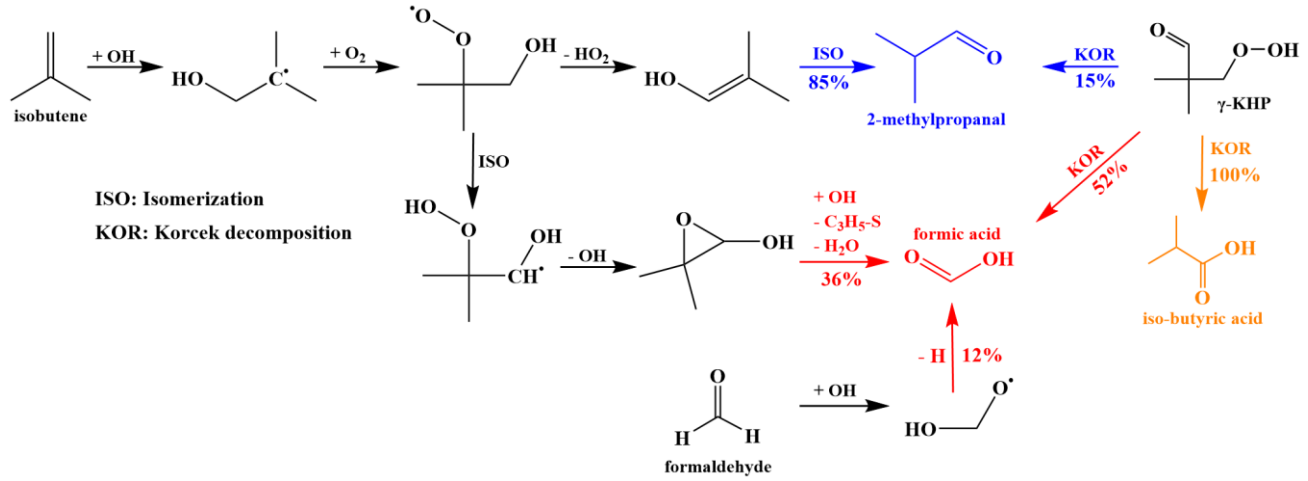

Scheme 4 The reaction pathway analysis for 2-methylpropanal, formic acid, and iso-butyric acid at φ = 0.5 and 650 K. The numbers represent the contribution of each reaction channel to the formation of 2-methylpropanal, formic acid, and iso-butyric acid, respectively. Only the main reaction pathways are shown here.

In addition, acetic acid was measured in this work. This carboxylic acid could not be formed by the Korcek decomposition of the C_5 γ-KHP in neopentane oxidation. Carboxylic acids are often observed in combustion experiments,[23,48] and there have been some exploratory studies on their formation during low temperature oxidation.[33,36,49] Battin-Leclerc et al.[49] proposed possible channels for the formation of short-chain monocarboxylic acids, e.g., C_1–C_3 carboxylic acids that are mainly formed from aldehydes with the same structure. In this work, the reaction of ȮH radical addition to aldehydes and the subsequent decomposition via C–H bond scission--Scheme 2 (3) was added to the model. Furthermore, an additional formation pathway of acetic acid was proposed in this work, i.e., the reaction of ȮH radical addition to acetone and the subsequent decomposition--Scheme 2 (4). Experimental measured and model-predicted mole fraction profiles of acetic acid are shown in Fig. 3f. Compared to NUIGMech1.2,[29] the current model has significantly improved the mole fractions of acetic acid.

4.2.3 Other products from neopentane oxidation

Other key products of neopentane oxidation were also identified and quantified in this work. The measured and model-predicted mole fraction profiles of ethylene, propene, methanol, ketene, acetaldehyde, methacrolein, hydrogen peroxide, and methyl hydroperoxide at $\varphi = 0.5$ are shown in Fig. 4. For these key species, the predictions from the updated model improved significantly, especially under the conditions of $\varphi = 0.9$ and $\varphi = 1.62$, as shown in Fig. S2. The model predicts well the formation of ethylene and propene under this condition. The simulations show that both ethylene and propene are mainly derived from the H-atom abstraction reaction and subsequent reactions of isobutene. In addition, ketene and methacrolein are also mainly derived from isobutene. Methoxy radicals are the main precursors of methanol, which are dominantly formed from O–O bond scission of methyl hydroperoxide. For methyl hydroperoxide, methyl radical addition to O_2 and subsequent reaction of $CH_3\dot{O}_2$ with $H\dot{O}_2$ radical is responsible for its formation. The model overpredicts the mole fraction of methanol by a factor of two; this overprediction may be caused by the overprediction of methyl hydroperoxide by the model. We note that the model predicts the mole fraction profiles of methanol and methyl hydroperoxide well at $\varphi = 0.9$ and $\varphi = 1.62$. Acetaldehyde is an important intermediate with a wide range of sources, in which C_5 KHP decomposition and subsequent reactions are one of the dominant formation pathways. For acetaldehyde, SVUV-PIMS data are in good agreement with the prediction by the updated model, but the GC data are lower than SVUV-PIMS data by a factor of two at $\varphi = 0.5$, $\varphi = 0.9$, and $\varphi = 1.62$. Hydrogen peroxide plays an important role in low temperature oxidation. The model results show that hydrogen peroxide is mainly produced by the disproportionation reaction of two $H\dot{O}_2$ radicals and the H-atom abstraction reaction from neopentane by $H\dot{O}_2$ radicals and is mainly consumed by decomposing into two $\dot{O}H$ radicals. The model overpredicts the mole fraction of hydrogen peroxide by a factor of 1.5 at $\varphi = 0.5$, but underpredicts its mole fraction profiles by a factor of 2 at $\varphi = 0.9$ and well predicts its mole fraction profiles at $\varphi = 1.62$.

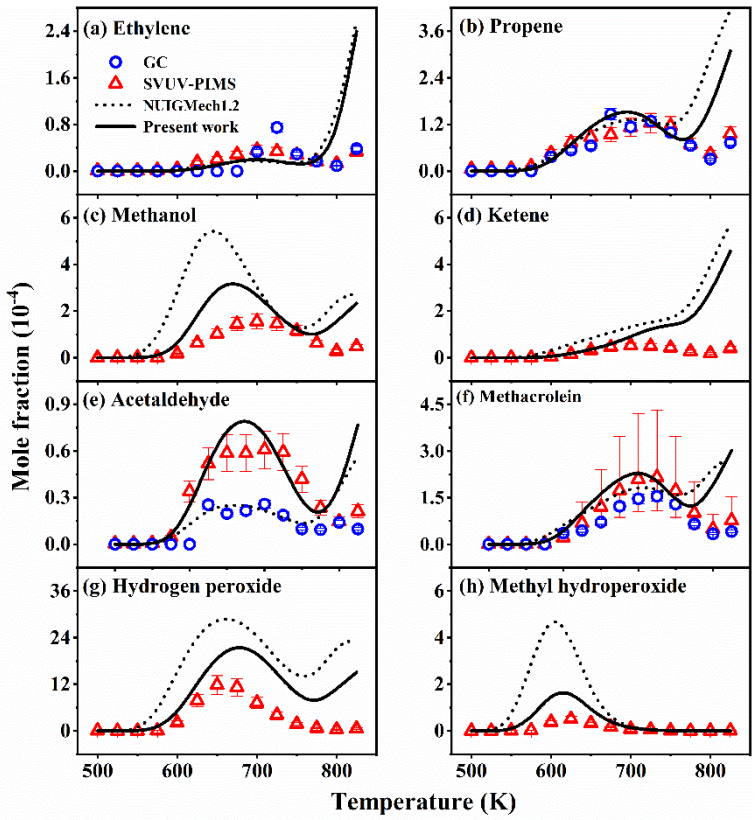

Figure 4 Measured (symbols) and model-predicted (lines) mole fraction profiles of ethylene, propene, methanol, ketene, acetaldehyde, methacrolein, hydrogen peroxide, and methyl hydroperoxide at φ = 0.5. The dotted and solid lines represent the results predicted by NUIGMech1.2[29] and the present model, respectively. The error bar for the experimental data is given.

The additional validation results based on this model can be found in the *supplementary materials*, including JSR species data measured at high temperatures, other JSR speciation data measured in this work, and IDTs of both STs and RCMs. Overall, the updated model in this work satisfactorily predicts these experimental data.

5. Summary and conclusions

In this work, two different analytical methods (SVUV-PIMS and GC) were used to investigate neopentane oxidation in JSRs at 1 atm and three different equivalence ratios of 0.5, 0.9, and 1.62. The experimental data obtained by different analytical methods are in good agreement; these different analytical methods complement each other, making the experimental results more comprehensive. Numerous important intermediates were identified and quantified, e.g., acetone, 3,3-dimethyloxetane, methacrolein, isobutene, 2-methylpropanal, formic acid, iso-butyric acid, acetic acid, methyl

hydroperoxide, and hydrogen peroxide. These key intermediates are crucial for clarifying the low temperature oxidation mechanism of neopentane and developing the kinetic model.

An updated kinetic model is proposed based on the current experimental data and previous neopentane studies. The pressure dependence of the reaction classes of $\dot{Q}OOH + O_2$ and $\dot{Q}OOH$ decompositions was considered, which is important for improving the predictions under atmospheric conditions. The identification of iso-butyric acid supports the existence of the Korcek mechanism during neopentane oxidation, which is consistent with the point proposed by Bourgalais et al.[21] and Eskola et al.[19] The Korcek reactions were added to the updated kinetic model. However, the results show that the Korcek reactions could not fully explain the experimental observations. Regarding the formation of acetic acid, the reaction pathways of ȮH radical addition to acetone/acetaldehyde and subsequent reactions were considered. The model analysis shows that the reaction pathway of ȮH radical addition to acetone and the subsequent decomposition is the most dominant formation channel of acetic acid.

The updated kinetic model was well validated against the speciation data measured in this work and various experimental data available in the literature, including IDTs of both STs and RCMs and JSR species data measured at high temperatures. We note that further improvement of the neo-pentane model is still needed to reduce model uncertainty, including quantum calculations of the newly added reaction pathways discussed in the current study. This model could provide a valuable reference for further updating alkane kinetic models or exploring the low temperature oxidation chemistry of highly branched alkanes.

Supporting Information

Additional validation results and an updated kinetic model of neopentane oxidation are provided.

Acknowledgements

This work was supported by National Natural Science Foundation of China (51976208) and the Hefei Science Center, CAS (2020HSC-KPRD001, 2021HSC-UE005).

References

(1) Sun, W.; Gao, X.; Wu, B.; Ombrello, T. The effect of ozone addition on combustion: Kinetics and dynamics. *Progr. Energy Combust. Sci.* **2019**, *73*, 1-25.

(2) Manente, V.; Johansson, B.; Cannella, W. Gasoline partially premixed combustion, the future of internal combustion engines? *Int. J. Engine Res.* **2011**, *12* (3), 194-208.

(3) Reitz, R. D.; Duraisamy, G. Review of high efficiency and clean reactivity controlled compression ignition (RCCI) combustion in internal combustion engines. *Progr. Energy Combust. Sci.* **2015**, *46*, 12-71.

(4) Yao, M.; Zheng, Z.; Liu, H. Progress and recent trends in homogeneous charge compression ignition (HCCI) engines. *Progr. Energy Combust. Sci.* **2009**, *35* (5), 398-437.

(5) Agarwal, A. K.; Singh, A. P.; Maurya, R. K. Evolution, challenges and path forward for low temperature combustion engines. *Progr. Energy Combust. Sci.* **2017**, *61*, 1-56.

(6) Jia, M.; Xie, M.; Wang, T.; Peng, Z. The effect of injection timing and intake valve close timing on performance and emissions of diesel PCCI engine with a full engine cycle CFD simulation. *Appl. Energy* **2011**, *88* (9), 2967-2975.

(7) Jia, M.; Li, Y.; Xie, M.; Wang, T. Numerical evaluation of the potential of late intake valve closing strategy for diesel PCCI (premixed charge compression ignition) engine in a wide speed and load range. *Energy* **2013**, *51*, 203-215.

(8) Wang, Z.; Popolan-Vaida, D. M.; Chen, B.; Moshammer, K.; Mohamed, S. Y.; Wang, H.; Sioud, S.; Raji, M. A.; Kohse-Hoinghaus, K.; Hansen, N.; et al. Unraveling the structure and chemical mechanisms of highly oxygenated intermediates in oxidation of organic compounds. *Proc. Natl. Acad. Sci. U. S. A.* **2017**, *114* (50), 13102-13107.

(9) Wang, Z.; Herbinet, O.; Hansen, N.; Battin-Leclerc, F. Exploring hydroperoxides in combustion: History, recent advances and perspectives. *Progr. Energy Combust. Sci.* **2019**, *73*, 132-181.

(10) Wang, Z.; Mohamed, S. Y.; Zhang, L.; Moshammer, K.; Popolan-Vaida, D. M.; Shankar, V. S. B.; Lucassen, A.; Ruwe, L.; Hansen, N.; Dagaut, P.; et al. New insights into the low-temperature oxidation of 2-methylhexane. *Proc. Combust. Inst.* **2017**, *36* (1), 373-382.

(11) Wang, Z.; Zhang, L.; Moshammer, K.; Popolan-Vaida, D. M.; Shankar, V. S. B.; Lucassen, A.; Hemken, C.; Taatjes, C. A.; Leone, S. R.; Kohse-Höinghaus, K.; et al. Additional chain-branching pathways in the low-temperature oxidation of branched alkanes. *Combust. Flame* **2016**, *164*, 386-396.

(12) Wang, Z.; Sarathy, S. M. Third O_2 addition reactions promote the low-temperature auto-ignition of n-alkanes. *Combust. Flame* **2016**, *165*, 364-372.

(13) Baker, R. R.; Baldwin, R. R.; Walker, R. W. Addition of neopentane to slowly reacting mixtures of $H_2 + O_2$ at 480°C. Part II. The addition of the primary products from neopentane, and the rate constants for H and OH attack on neopentane. *Combust. Flame* **1976**, *27*, 147-161.

(14) Curran, H. J.; Pit, W. J.; Westbrook, C. K.; Hisham, M. W. M.; Walker, R. W. An intermediate temperature modeling study of the combustion of neopentane. *Symp. (Int.) Combust.* **1996**, *26* (1), 641-649.

(15) Wang, S.; Miller, D. L.; Cernansky, N. P.; Curran, H. J.; Pitz, W. J.; Westbrook, C. K. A flow reactor study of neopentane oxidation at 8 atmospheres: Experiments and modeling. *Combust. Flame* **1999**, *118* (3), 415-430, Article.

(16) Dagaut, P.; Cathonnet, M. Oxidation of neopentane in a jet-stirred reactor from 1 to 10 atm: an experimental and detailed kinetic modeling study. *Combust. Flame* **1999**, *118* (1), 191-203.

(17) Bugler, J.; Marks, B.; Mathieu, O.; Archuleta, R.; Camou, A.; Grégoire, C.; Heufer, K. A.; Petersen, E. L.; Curran, H. J. An ignition delay time and chemical kinetic modeling study of the pentane isomers. *Combust. Flame* **2016**, *163*, 138-156.

(18) Bugler, J.; Somers, K. P.; Silke, E. J.; Curran, H. J. Revisiting the Kinetics and Thermodynamics of the Low-Temperature Oxidation Pathways of Alkanes: A Case Study of the Three Pentane Isomers. *J. Phys. Chem. A* **2015**, *119* (28), 7510-7527.

(19) Eskola, A. J.; Antonov, I. O.; Sheps, L.; Savee, J. D.; Osborn, D. L.; Taatjes, C. A. Time-resolved measurements of product formation in the low-temperature (550-675 K) oxidation of neopentane: a probe to investigate chain-branching

mechanism. *Phys. Chem. Chem. Phys.* **2017**, *19* (21), 13731-13745.

(20) Hansen, N.; Kukkadapu, G.; Chen, B.; Dong, S.; Curran, H. J.; Taatjes, C. A.; Eskola, A. J.; Osborn, D. L.; Sheps, L.; Pitz, W. J.; et al. The impact of the third O_2 addition reaction network on ignition delay times of neo-pentane. *Proc. Combust. Inst.* **2021**, *38* (1), 299-307.

(21) Bourgalais, J.; Herbinet, O.; Carstensen, H.-H.; Debleza, J.; Garcia, G. A.; Arnoux, P.; Tran, L. S.; Vanhove, G.; Liu, B.; Wang, Z.; et al. Jet-Stirred Reactor Study of Low-Temperature Neopentane Oxidation: A Combined Theoretical, Chromatographic, Mass Spectrometric, and PEPICO Analysis. *Energy Fuels* **2021**, *35* (23), 19689-19704.

(22) Xu, Q.; Liu, B.; Chen, W.; Yu, T.; Zhang, Z.; Zhang, C.; Wei, L.; Wang, Z. Comprehensive study of the low-temperature oxidation chemistry by synchrotron photoionization mass spectrometry and gas chromatography. *Combust. Flame* **2022**, *236*.

(23) Herbinet, O.; Battin-Leclerc, F.; Bax, S.; Le Gall, H.; Glaude, P. A.; Fournet, R.; Zhou, Z.; Deng, L.; Guo, H.; Xie, M.; et al. Detailed product analysis during the low temperature oxidation of n-butane. *Phys. Chem. Chem. Phys.* **2011**, *13* (1), 296-308.

(24) Photonionization cross section database (Version 2.0), National Synchrotron Radiation Laboratory, Hefei, China **2017**, http://flame.nsrl.ustc.edu.cn/en/database.htm.

(25) Dodson, L. G.; Shen, L.; Savee, J. D.; Eddingsaas, N. C.; Welz, O.; Taatjes, C. A.; Osborn, D. L.; Sander, S. P.; Okumura, M. VUV photoionization cross sections of HO_2, H_2O_2, and H_2CO. *J. Phys. Chem. A* **2015**, *119* (8), 1279-1291.

(26) Moshammer, K.; Jasper, A. W.; Popolan-Vaida, D. M.; Wang, Z.; Bhavani Shankar, V. S.; Ruwe, L.; Taatjes, C. A.; Dagaut, P.; Hansen, N. Quantification of the Keto-Hydroperoxide ($HOOCH_2OCHO$) and Other Elusive Intermediates during Low-Temperature Oxidation of Dimethyl Ether. *J. Phys. Chem. A* **2016**, *120* (40), 7890-7901.

(27) Herbinet, O.; Husson, B.; Serinyel, Z.; Cord, M.; Warth, V.; Fournet, R.; Glaude, P.-A.; Sirjean, B.; Battin-Leclerc, F.; Wang, Z.; et al. Experimental and modeling investigation of the low-temperature oxidation of n-heptane. *Combust. Flame* **2012**, *159* (12), 3455-3471.

(28) Wang, Z.; Herbinet, O.; Cheng, Z.; Husson, B.; Fournet, R.; Qi, F.; Battin-Leclerc, F. Experimental investigation of the low temperature oxidation of the five isomers of hexane. *J. Phys. Chem. A* **2014**, *118* (30), 5573-5594.

(29) Dong, S.; Aul, C.; Gregoire, C.; Cooper, S. P.; Mathieu, O.; Petersen, E. L.; Rodriguez, J.; Mauss, F.; Wagnon, S. W.; Kukkadapu, G.; et al. A comprehensive experimental and kinetic modeling study of 1-hexene. *Combust. Flame* **2021**, *232*.

(30) Goldsmith, C. F.; Green, W. H.; Klippenstein, S. J. Role of O_2 + QOOH in low-temperature ignition of propane. 1. Temperature and pressure dependent rate coefficients. *J. Phys. Chem. A* **2012**, *116* (13), 3325-3346.

(31) Duan, J.; Ji, J.; Ye, L.; Zhai, Y.; Zhang, L. A theoretical kinetics study on low-temperature oxidation of *n*-C_4H_9 radicals. *Proc. Combust. Inst.* **2021**, *38* (1), 681-689.

(32) Duan, J.; Ji, J.; Ye, L.; Meng, Q.; Zhai, Y.; Zhang, L. Theoretical calculation of low-temperature oxidation of heptyl radicals and O_2. *Combust. Flame* **2020**, *217*, 274-284.

(33) Jalan, A.; Alecu, I. M.; Meana-Paneda, R.; Aguilera-Iparraguirre, J.; Yang, K. R.; Merchant, S. S.; Truhlar, D. G.; Green, W. H. New pathways for formation of acids and carbonyl products in low-temperature oxidation: the Korcek decomposition of γ-ketohydroperoxides. *J. Am. Chem. Soc.* **2013**, *135* (30), 11100-11114.

(34) Ranzi, E.; Cavallotti, C.; Cuoci, A.; Frassoldati, A.; Pelucchi, M.; Faravelli, T. New reaction classes in the kinetic modeling of low temperature oxidation of n-alkanes. *Combust. Flame* **2015**, *162* (5), 1679-1691.

(35) Zhang, K.; Banyon, C.; Bugler, J.; Curran, H. J.; Rodriguez, A.; Herbinet, O.; Battin-Leclerc, F.; B'Chir, C.; Heufer, K. A. An updated experimental and kinetic modeling study of n-heptane oxidation. *Combust. Flame* **2016**, *172*, 116-135.

(36) Goldsmith, C. F.; Burke, M. P.; Georgievskii, Y.; Klippenstein, S. J. Effect of non-thermal product energy distributions on ketohydroperoxide decomposition kinetics. *Proc. Combust. Inst.* **2015**, *35* (1), 283-290.

(37) Xu, S.; Zhu, R. S.; Lin, M. C. Ab initio study of the OH + CH_2O reaction: The effect of the OH··OCH_2 complex on the H-abstraction kinetics. *Int. J. Chem. Kinet.* **2006**, *38* (5), 322-326.

(38) Zádor, J.; Miller, J. A. Unimolecular dissociation of hydroxypropyl and propoxy radicals. *Proc. Combust. Inst.* **2013**, *34* (1), 519-526.

(39) Yamada, T.; Taylor, P. H.; Goumri, A.; Marshall, P. The reaction of OH with acetone and acetone-d_6 from 298 to 832 K: Rate coefficients and mechanism. *J. Chem. Phys.* **2003**, *119* (20), 10600-10606.

(40) Henon; E.; Canneaux; S.; Bohr; F.; Dobe. Features of the potential energy surface for the reaction of OH radical with acetone. *Phys. Chem. Chem. Phys.* **2003**.

(41) Vasvári, G.; Szilágyi, I.; Bencsura, Á.; Dóbe´, S.; Be´rces, T.; Henon, E.; Canneaux, S.; Bohr, F. d. r. Reaction and complex formation between OH radical and acetone. *Phys. Chem. Chem. Phys.* **2001**, *3* (4), 551-555.

(42) Dong, B.; Hu, Z.; Xu, Q.; Liu, B.; Zhu, Q.; Guan, J.; Liu, C.; Pan, Y.; Hu, L.; Fang, J.; et al. Improving quantification of hydrogen peroxide by synchrotron vacuum ultraviolet photoionization mass spectrometry. *Combust. Flame* **2022**, 112214.

(43) Zhou, Z.; Xie, M.; Wang, Z.; Qi, F. Determination of absolute photoionization cross-sections of aromatics and aromatic derivatives. *Rapid Commun. Mass Spectrom.* **2009**, *23* (24), 3994-4002.

(44) CHEMKIN-PRO 15092, Reaction Design, San Diego, **2009**.

(45) Miyoshi, A. Systematic computational study on the unimolecular reactions of alkylperoxy (RO_2), hydroperoxyalkyl (QOOH), and hydroperoxyalkylperoxy (O_2QOOH) radicals. *J. Phys. Chem. A* **2011**, *115* (15), 3301-3325.

(46) Goldsmith, C. F.; Klippenstein, S. J.; Green, W. H. Theoretical rate coefficients for allyl+HO_2 and allyloxy decomposition. *Proc. Combust. Inst.* **2011**, *33* (1), 273-282.

(47) Sarathy, S. M.; Westbrook, C. K.; Mehl, M.; Pitz, W. J.; Togbe, C.; Dagaut, P.; Wang, H.; Oehlschlaeger, M. A.; Niemann, U.; Seshadri, K.; et al. Comprehensive chemical kinetic modeling of the oxidation of 2-methylalkanes from C_7 to C_{20}. *Combust. Flame* **2011**, *158* (12), 2338-2357.

(48) Wang, Z.; Chen, B.; Moshammer, K.; Popolan-Vaida, D. M.; Sioud, S.; Shankar, V. S. B.; Vuilleumier, D.; Tao, T.; Ruwe, L.; Bräuer, E.; et al. n-Heptane cool flame chemistry: Unraveling intermediate species measured in a stirred reactor and motored engine. *Combust. Flame* **2018**, *187*, 199-216.

(49) Battin-Leclerc, F.; Konnov, A. A.; Jaffrezo, J. L.; Legrand, M. To Better Understand the Formation of Short-Chain Acids in Combustion Systems. *Combust. Sci. Technol.* **2007**, *180* (2), 343-370.

TOC Graphic

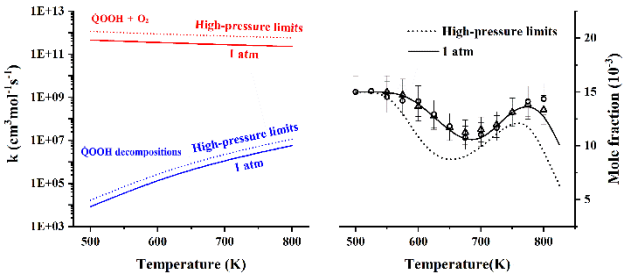
QOOH + O2
High-pressure limits
1 atm
QOOH decompositions
High-pressure limits
1 atm
k (cm3mol-1s-1)
Temperature (K)
High-pressure limits
1 atm
Mole fraction (10-3)
Temperature(K)